



Impact mechanism of gel's alkali circumstance on the morphologies and electrical properties of $\text{Ba}_{0.80}\text{Sr}_{0.20}\text{TiO}_3$ ceramics

Yongshang Tian¹ · Lijia Cao¹ · Zhijia Chen¹ · Yansheng Gong² · Yitian Tang¹ · Qiangshan Jing¹

Received: 23 November 2018 / Accepted: 2 March 2019 / Published online: 14 March 2019
© Springer Science+Business Media, LLC, part of Springer Nature 2019

Abstract

$\text{Ba}_{0.8}\text{Sr}_{0.2}\text{TiO}_3$ (BST) nanopowder was successfully synthesized by Pechini sol-gel method under different temperatures. Not only were BaCO_3 impurity phase production and transition temperature from cubic to tetragonal phase respectively set at 440 °C and 800 °C, but also barium (Ba) resided in a 12-coordinate site of crystal lattice was set at 580 °C by the techniques of X-ray diffraction (XRD) and Fourier transform infrared spectroscopy (FT-IR). In addition, gels at pH 3–8 were used to prepare BST ceramics and the ceramics morphology was characterized by scanning electron microscope (SEM). The interrelationship between morphology and electrical properties, which were associated with precipitation phase on the crystal boundary of BST ceramics, was studied in detail. Finally, the optimal electrical properties of the ceramics were comprehensively displayed in this work, i.e., $\epsilon_r = 8113.81$, $d_{33} = 78$ pC/N, $k_p = 14.96\%$, and $Q_m = 85.08$ at pH 5.

Graphical Abstract

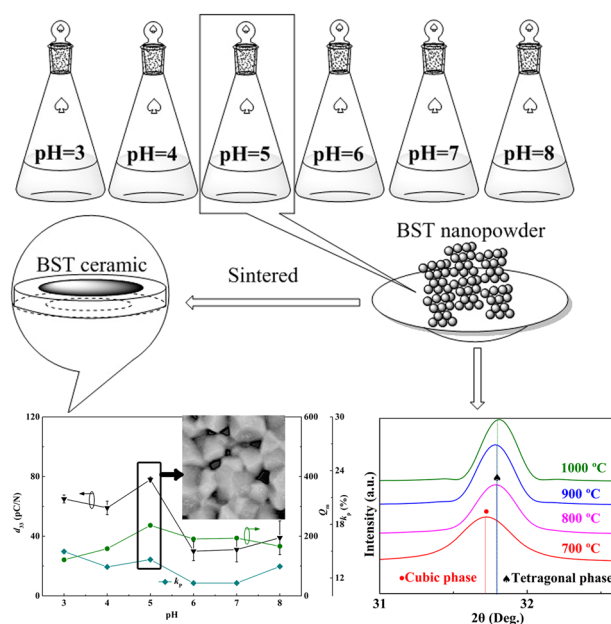
This research adopts Pechini sol-gel method for synthesis of $\text{Ba}_{0.8}\text{Sr}_{0.2}\text{TiO}_3$ (BST) nanopowder and solid-state reaction for preparation of BST ceramics. Cubic to tetragonal phase evolution of nanopowder is detected when temperature above 800 °C. The optimal electrical properties of the ceramics are obtained with the as-synthesized nanopowder when gels at pH 5. The meaningful results exhibit for tunable microwave application.

✉ Yongshang Tian
tianyongshang423@163.com
tianyongshang@xynu.edu.cn

✉ Qiangshan Jing
9jqshan@163.com

¹ College of Chemistry and Chemical Engineering, Henan Key Laboratory of Utilization of Non-metallic Mineral in the South of Henan, Xinyang Normal University, Xinyang 464000, People's Republic of China

² Faculty of Material Science and Chemistry, China University of Geosciences, Wuhan 430074, People's Republic of China



Highlights

1. Gelation and pyroreaction processes for $\text{Ba}_{0.8}\text{Sr}_{0.2}\text{TiO}_3$ nanopowder were studied.
2. Pyroreaction induced the nanopowder from cubic to tetragonal phase transition.
3. Ceramics were prepared by Pechini sol-gel method with different pH values.
4. Interrelationship of ceramics morphology and electrical properties was shown.

Keywords $\text{Ba}_{0.8}\text{Sr}_{0.2}\text{TiO}_3$ · pH · Pechini method · Morphology · Electrical properties

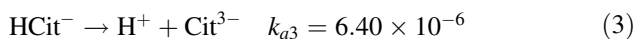
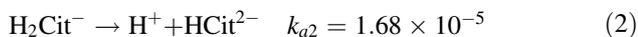
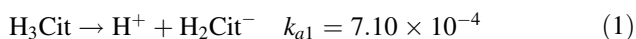
1 Introduction

Barium titanate (BT) ceramic with perovskite structure had been extensively studied for the primary electrical properties as well as ubiquity in piezoelectric materials [1]. Either isovalent or aliovalent modification in BT solid solution very often underlie the decrement on transition temperature and dielectric dissipation factors, and the increment on electrical properties [2]. It presented that barium strontium titanate solid solution had been diffusely applied into microwave devices including wireless communications (microwave phase shifter, delay lines dielectric filters, and voltage-controlled oscillators), varactors, multilayer ceramic capacitors, dynamic random access memories, etc [3–5]. Comparing with other divalent ions, strontium (Sr), which was doped in BT ceramic, had improved the piezoelectric coefficient (d_{33}) realistically [6]. Further, the high permittivity, low dielectric loss, and high d_{33} are needed for these tunable microwave applications [7, 8]. Besides, barium strontium titanate ceramic is deemed to be an irreplaceable member among lead-free piezoelectric ceramic whose electrical properties were comparable to lead-based ceramics [7, 9]. However, the permittivity and piezoelectric coefficients of barium strontium titanate ceramic are inferior

to lead-based ceramic for the moment, the Curie temperature (T_C) of barium strontium titanate based ceramic is lower than lead-based ceramic, and the thermal dynamic stabilization is unsatisfactory [10]. In this study, we aimed on pinpointing the optimal condition to prepare barium strontium titanate ceramic of highly admirable electrical properties.

There are several techniques to prepare barium strontium titanate ceramic, such as hydrothermal, co-precipitation, spray pyrolysis, reverse micelles, combustion, and sol-gel methods [11–13]. Pechini sol-gel method is considered as a representative part of sol-gel method [14]. It means that the liquid precursor should be prepared by metal salt, ethylene glycol, as well as citric acid under low-temperature, transformed into a sol, and finally to a gelatin [15]. In this work, $\text{Ba}_{0.8}\text{Sr}_{0.2}\text{TiO}_3$ (BST) nanopowder was synthesized by Pechini sol-gel method and ulteriorly sintered into ceramics under ordinary pressure. During sol formation process, the ionizing equilibrium of citric acid and the coordination equilibrium existed in solution compound of citric acid and metal ions. Act as a crucial raw material, citric acid's ionization equilibrium is enormously influenced by the pH condition of the solution compounds (Eqs. 1–3) [16]. The gelation process directly impacts the crystal phase structure

of BST nanopowder. Purity crystal phase structural nanopowder contributes to synthesize high tenability and high electrical property ceramics. Hence, pH conditions of the solution compounds and temperature condition for nanopowder were studied to obtain purity crystal phase structure BST nanopowder, improving the electrical properties of BST ceramic in this study.



2 Experimental

Ethylene glycol (Sinopharm Chemical Reagent Co., Ltd, 99.0% purity) and citric acid (Sinopharm Chemical Reagent Co., Ltd, 99.5% purity) were mixed by 4:1 ratio, accompanying with the magnetic stirring under the temperature of 55 °C. The $\text{Ti}(\text{OBU})_4$ (Sinopharm Chemical Reagent Co., Ltd, 98.0% purity) was added into the mixture as soon as the citric acid was completely dissolved to make homogeneous modified precursor. The polycondensation reaction was affirmed to end after 3 h stirring. Then Barium acetate (Sinopharm Chemical Reagent Co., Ltd, 99.0% purity) and strontium nitrate (Sinopharm Chemical Reagent Co., Ltd, 99.5% purity) were co-doped into the precursor successively. After stirring for 1 h, the solution process finished. Under the temperature of 110 °C, the sol was oven dried for 24 h. Furthermore, the structurally stable gel was formed after 12 h maturing under the room temperature. The weight loss and differential thermal analysis of gel (dried at 200 °C) were measured in a Thermogravimetric analysis/differential scanning calorimeter (TG/DSC, NETZSCH, STA 449 F5, DE) from room temperature to 1200 °C. The crucibles of gelatin were calcined into dark brown powder under the temperature from 350 °C to 470 °C in the furnace with the confirmed procedure. In addition, 440 °C was confirmed to be the calcination temperature for dark brown powder. Next, they were calcined into nanopowder under the temperature designated from 500 °C to 1000 °C. In order to illuminate the phase and component transitions of the powder, we adopted X-ray diffraction (XRD, Mini Flex 600), and Fourier transform infrared spectroscopy (FT-IR, Nicolet IS-50) for mutual corroboration.

After exploring the temperature for both reaction and grain growth process in the nanopowder, the impacts of pH conditions on structure and electrical properties were also investigated. The gels at pH 3–8 were characterized by a

precise pH instrument (pHS-3C, INESA). These gels were processed as nanopowder under the same temperatures mentioned before. After that, the discs, 1 mm diameter and 1.5 mm thickness, were pressed under a 20 MPa pressure intensity using polyvinyl alcohol (PVA) of 5–6 wt.% as a binder. PVA was burned off at 650 °C for 2 h. Then the samples were sintered at 1260 °C for 4 h and the heating and cooling rates are respectively 3 and 4 °C/min. For the measurement of electrical properties, silver slurry firing on both sides of the sintered ceramics was under 570 °C for 12 min [17]. The permittivity (ϵ_r) and dielectric loss ($\tan \delta$) were both tested at room temperature under regularly different frequencies by a LCR analyzer (E4900A, Keysight). The ϵ_r and $\tan \delta$ were tested at the frequency 10 kHz further by a precision impedance analyzer (Wayne Kerr) from 30 °C to 200 °C. BST ceramics were poled by a polarization installation (HYJH-4-5) under room temperature in a silicone oil bath for 40 min when dc field achieved to 3 kV/min. Twenty-four hours after poling, the piezoelectric constants of the ceramics were measured by piezo- d_{33} meter (ZJ-3AN). The d_{33} , which were measured by the LCR analyzer (E4900A, Keysight), were used to calculate mechanic quality factor (Q_m) and electromechanical coupling factor (k_p) with the Onoe and Jumonji's empirical Eqs. 4 and 5 [18]. Finally, the morphology on natural section of the ceramics was shown by scanning electron microscope (SEM, S-4800).

$$k_p = \frac{1}{\sqrt{0.395 \times \frac{f_a}{(f_a - f_r)} + 0.574}} \quad (4)$$

$$Q_m = \frac{1}{2 \times \pi \times f_{r \times Z_{\min} \times C^T} \times \left[1 - \left(\frac{f_a}{f_r}\right)^2\right]} \quad (5)$$

3 Results and discussion

3.1 Reaction process

3.1.1 Gelation process

As a precursor in hydrolysis, $\text{Ti}(\text{OBU})_4$ continuously reacts with H_2O until $\text{Ti}(\text{OH})_4$ produced. In order to reduce rate of hydrolysis and obtain stable sol, the citric acid combined with the $\text{Ti}(\text{OBU})_4$ precursor as a chelating agent to form complexes with large steric hindrance [19]. For the sake of building a reticulate polymer, the dehydration polycondensation reaction and the dealcoholization polycondensation reaction are set off simultaneously. When the polycondensation reaction have accomplished, the metal

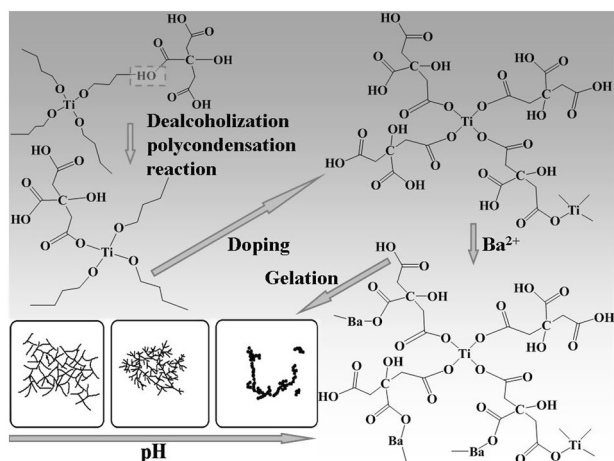


Fig. 1 The reaction process of Pechini sol-gel method

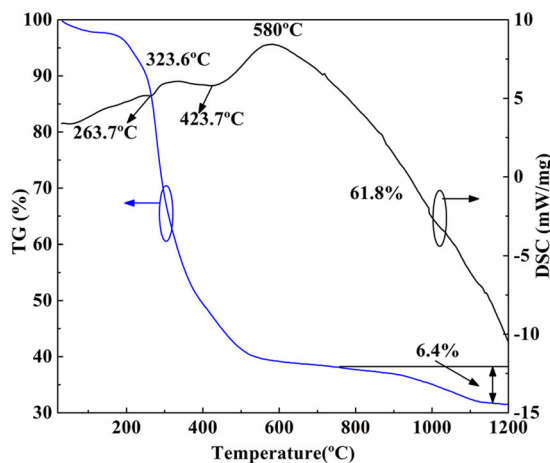


Fig. 2 TG/DSC curves of BST gel

ions are doped into the reticulate structure, which are combined with bridging oxygen bonds as Ti-O-Ti, Ba-O-Ba, and Sr-O-Sr. The water and organic solution still existed in the sol. During the aging process, the reticulate structure is starting to shrink, the condensation polymerization is keeping on, and the solution may lose at the same time [15]. That is the beginning of gelation procedure. According to the same mentality, the energy of citric acid in the combination with precursor is weakening as pH conditions increasing. Meanwhile, some of $\text{Ti}(\text{OBU})_4$ reprecipitates in the reticulate structure and the particles are contacted with each other to present one-dimensional linear structure, as shown in Fig. 1. It is useless to form stable solid solution and fine nanopowder.

Given this fact, some effects of different parameters, such as pH condition of gel and the calcination temperature, exist on morphology and particle size of products [20, 21]. As a consequence, the pH of gel strongly affects the

agglomeration product and ulteriorly affects the electrical or optical properties, etc.

3.1.2 Pyroreaction process

The gelatin samples (dried under the temperature of $200\text{ }^\circ\text{C}$) were measured by TG/DSC to investigate the pyroreaction decomposition behaviors of the modified precursor in air and the results were shown in Fig. 2. From room temperature to $263.7\text{ }^\circ\text{C}$, a minor weight loss in TG curve accompanied with a weak endothermic peak in DSC curve in virtue of water evaporating decalescence [21]. It was clearly shown in the DSC curve that the first exothermic peak was detected at $323.6\text{ }^\circ\text{C}$ with severe weight loss. Obviously, when the combustion stage was achieved, the polymer organics started to vaporize at $263.7\text{ }^\circ\text{C}$ [22]. As the temperature elevated to $440\text{ }^\circ\text{C}$, the second endothermic peak had been discovered. In the mean time, the impurity phase was detected. The final exothermic peak at $580\text{ }^\circ\text{C}$ showed that Ba-O and the impurity phase started to decompose. It was corroborated by the analysis of the FT-IR spectra and XRD patterns at a later stage [23]. Ultimately, Ba resided in a 12-coordinate site in the perovskite structure. In this conclusion, several temperatures that were adjacent to the temperatures mentioned before were selected to create powder and ceramics. The characterization of nanopowder that was calcined under the temperature from $55\text{ }^\circ\text{C}$ to $1000\text{ }^\circ\text{C}$ was accomplished.

The FT-IR spectra were shown in Fig. 3. The gels were created at $55\text{ }^\circ\text{C}$, dried at $200\text{ }^\circ\text{C}$, and respectively calcined into the dark brown powder from $200\text{ }^\circ\text{C}$ to $470\text{ }^\circ\text{C}$. After that, the dark brown powders were calcined into nanopowders respectively from $500\text{ }^\circ\text{C}$ to $1000\text{ }^\circ\text{C}$. The peaks ranged from 450 to 1000 cm^{-1} was identified to be three different kinds of vibration modes with TiO_6 octahedral structures, which involved the Ti-O_I stretching normal vibrations, Ti-O_{II} ending normal vibrations, and TiO_6 stretching vibration connected with barium [24]. Thus, the absorbance peaks of Ti-O at 503 cm^{-1} were detected and Ba-O (Fig. 3a) were detected around 423 and 856 cm^{-1} [25, 26]. The absorbance peaks were detected in frequency regime 1420 – 1600 cm^{-1} and the peaks at 1425 and 1565 cm^{-1} were identified to the asymmetrical and symmetrical vibration modes of (COO^-) carboxyl group, respectively [24]. These groups might exist as ligands in the chelating agents due to the complexation reaction between citric acid and $\text{Ti}(\text{OBU})_4$ [27]. It was proved that the absorbance peaks in the range of 1000 – 1100 cm^{-1} might have the $-\text{OR}$ groups in the combination between chelating agent and ions. The absorbance peaks of metal bridge oxygen bonds, such as Sr-O-Ti, Ba-O-Ti, and Ti-O-Ti, etc. range from 1300 to 1500 cm^{-1} [28]. It was evidently detected that the $(-\text{OH})$ groups had vaporized when the temperature

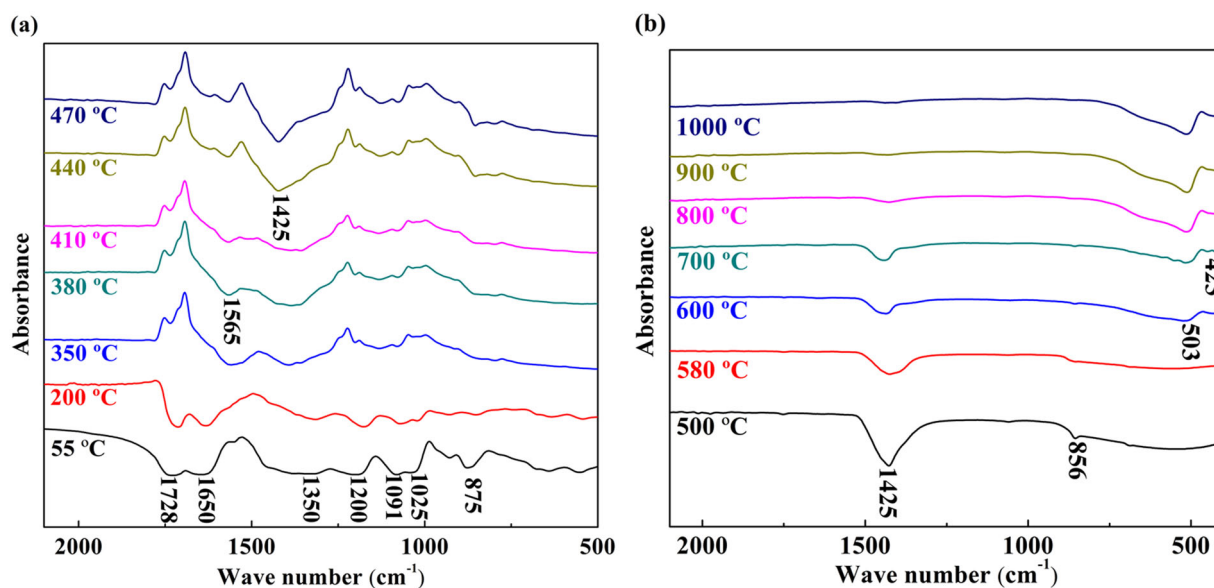


Fig. 3 FT-IR spectra of gels created at 55 °C and dried at 200 °C; FT-IR spectra of nanopowder calcined from 350 to 1000 °C (3(a) and 3(b))

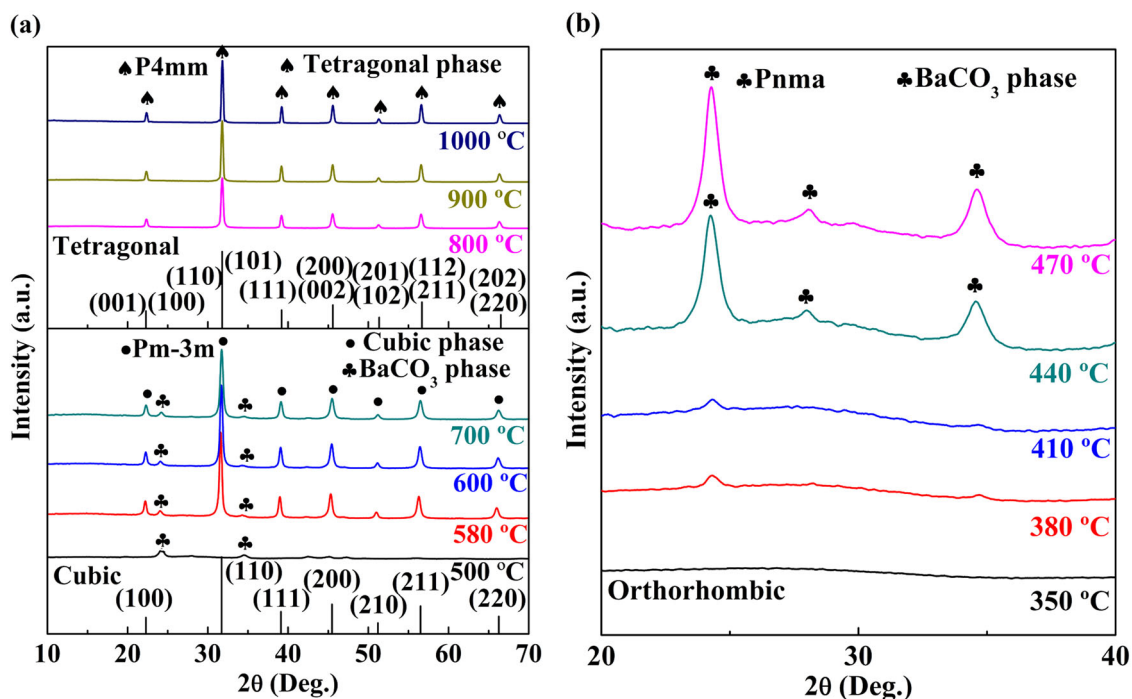
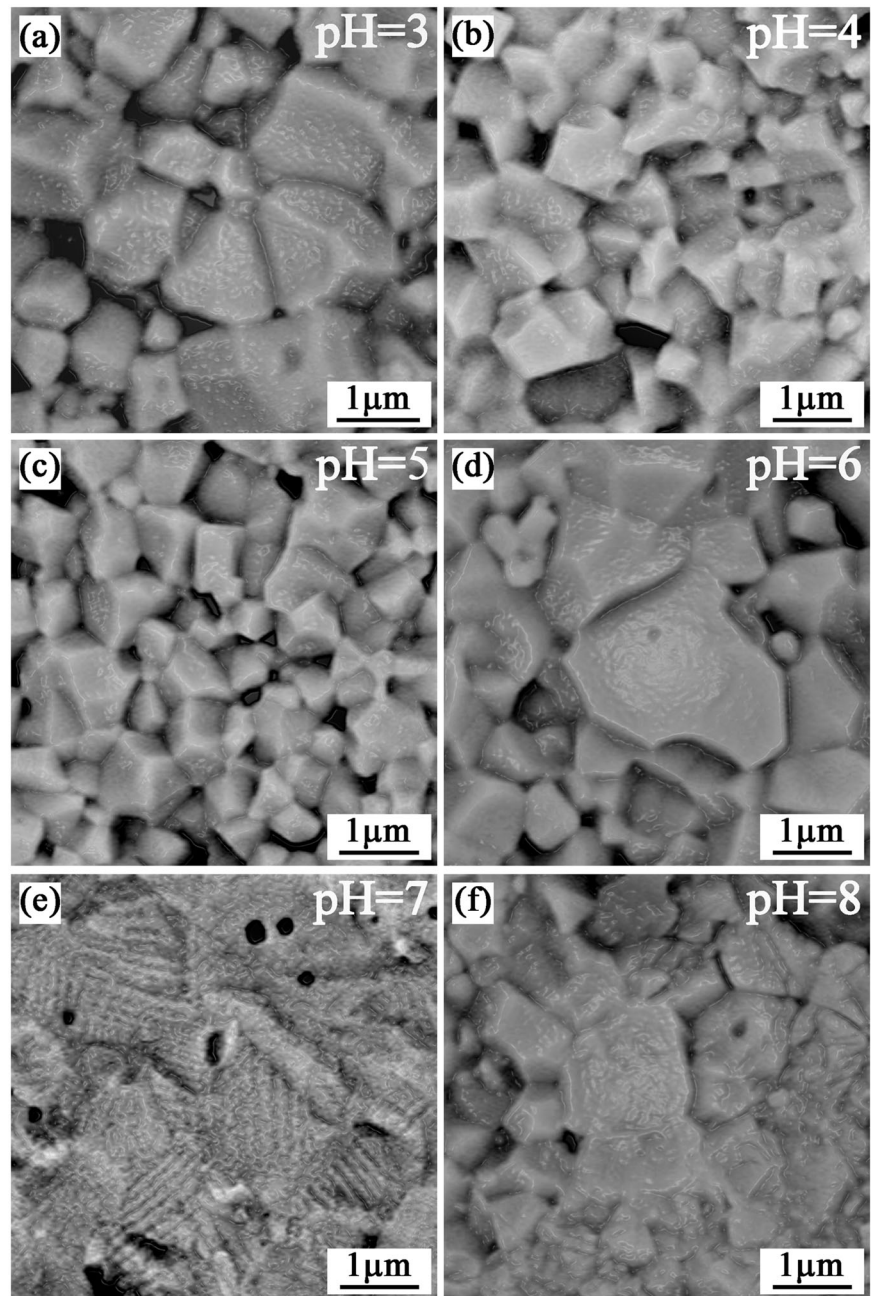


Fig. 4 XRD patterns of the nanopowder samples were calcined under the temperature from 500 to 1000 °C, and the dark brown powder samples were calcined under the temperatures from 350 to 470 °C

achieved to 440 °C. The absorbance peaks of (COO⁻) carboxyl group, which were considered as an impurity phase (mentioned in Fig. 4), appeared in FT-IR peaks simultaneously (mentioned in Fig. 3b). From 55 °C to 700 °C, there was always keeping Ba-O in FT-IR graph at the wave number of 856–875 cm⁻¹ [29]. In addition, the exothermic

peak, detected at 580 °C (mentioned in Fig. 2), was authenticated to be the transformation for Ba-O from compound to crystal lattice (mentioned in Fig. 4). As the calcination temperature arising at 800 °C, the absorbance peaks of impurity phase and Ba-O were disappeared completely (mentioned in Fig. 3b). The results shown in the FT-

Fig. 5 The morphology of BST ceramics prepared by gels under different pH conditions



IR graphs could be appropriately corresponded to the information in TG-DSC curves.

3.2 Structural studies

3.2.1 X-ray diffraction

The powder samples also characterized the phase transition under different calcination temperature conditions to confirm the phenomenon in FT-IR graphs and identify the optimal calcinations temperature ulteriorly. Figure 4 showed the XRD patterns of BST powder samples. In the

Fig. 4a, all the major diffraction peaks were indexed according to the standard XRD patterns of the cubic BST phase (Pm-3m, cubic phase) and an impurity phase both transformed into the tetragonal BST phase (P4mm, tetragonal phase) by Jade 6.0 software. In Fig. 4b, the impurity phase, which was identified to be BaCO₃ phase (Pnma, orthorhombic phase), was detected at 440 °C [30]. Meanwhile, BaCO₃ phase (Pnma, orthorhombic phase) disappeared at 800 °C. In Fig. 4a, the types of phase included cubic BST and the BaCO₃ impurity phase at 700 °C. There was no impurity phase observed and the principle crystal phase transformed from cubic to tetragonal phase as soon as

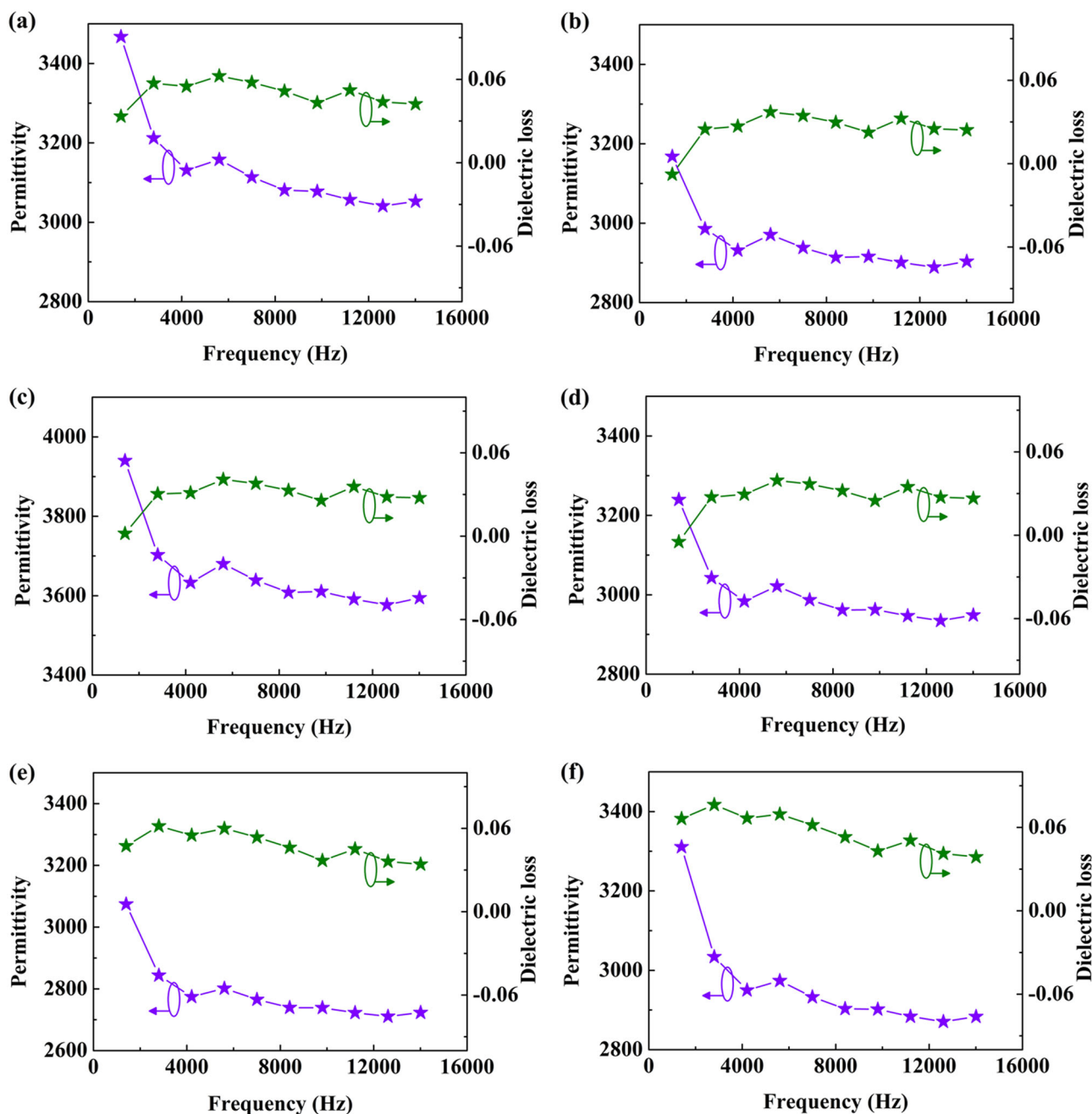


Fig. 6 ϵ_r and $\tan \delta$ vs. different frequencies of ceramics created by gels at pH 3–8. (6(a)–6(f))

the calcination temperature achieved 800 °C. The phenomenon was corresponding to the same things shown in FT-IR spectra. The BaCO_3 impurity phase appeared at 440 °C and had an absorbance peak at the wave number of 1425 cm^{-1} in FT-IR spectra. It was disappeared at 800 °C when the absorbance peak of BaCO_3 impurity phase disappeared at the same time. Furthermore, the absorbance of Sr-O-Ti vanished when the calcination temperature achieved 500 °C, but the diffraction peaks of BST phase still existed. It could be concluded that Sr^{2+} ions had dissolved in BaTiO_3

matrix and formed a stable BST crystal phase structure. Thus, there was no doubt that the optimal temperatures for calcinations of dark brown powder and nanopowder were respectively set at 440 and 800 °C.

3.2.2 Scanning electron microscopy

The SEM images of the fractured surface morphology were shown in Fig. 5. The average grain size was estimated by linear intercept method. The average grain size was

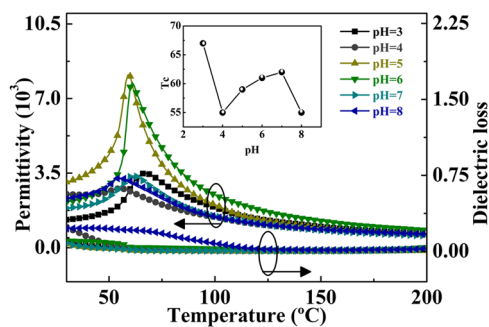


Fig. 7 ϵ_r and $\tan \delta$ vs. 10 kHz under different temperature of ceramics created by gels at pH 3–8

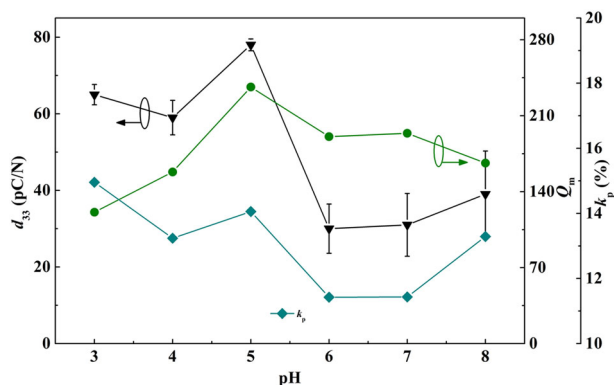


Fig. 8 d_{33} , Q_m , and k_p of polarized BST ceramics under different pH conditions of gels

graduated as 1.17, 0.63, 0.50, and 1.25 μm , respectively, from Fig. 5a, d. Moreover, from Fig. 5a, c, it was observed that the grain size of the ceramics became smaller and more regular. The minimum grain size was detected at Fig. 5c. At pH 6–8, the grain size of nanopowder increased, the crystal boundaries of the ceramics grew blurred, and the section of ceramics even displayed intergranular fracture [31, 32]. These kinds of phenomenon in the ceramics were closely related to the structure of gels, which were prepared under different pH conditions. As mentioned previously, alkaline gels could engender the reprecipitation on the molecular reticulate structure and ulteriorly a linear aggregation. This kind of aggregation experienced the calcination and sintering procedure, and formed a precipitated phase on the crystal boundaries [33]. Furthermore, with increment of gel's pH values, the situation of precipitated phase became more incurable and the intergranular fracture was detected in Fig. 5e, f.

3.3 Electrical properties

It was ulteriorly approved that the electrical properties and morphology of BST ceramics were influenced by crystal phase structure of BST nanopowder, which were prepared from gels at pH 3–8. The variation tendency of the ϵ_r and

$\tan \delta$ of BST ceramics are shown in Fig. 6 as the form of ϵ_r -frequency patterns from Fig. 6a, f. Both permittivity and dielectric loss of the BST ceramics were measured under incremental frequencies [34]. It showed that the decrement of ϵ_r and the fluctuation of $\tan \delta$ were followed with the increment of frequency. The decrement of ϵ_r was attributed to the jumping frequency of electric charge carriers in the samples that could not follow the alternation of the applied AC electric field beyond a certain critical frequency [35]. This tendency of dielectric and relaxation polarization mechanisms was generally detected at high frequencies. The ϵ_r value of piezoelectric material depended on the mobility of domain walls and the population of domains [36]. Consequently, the increment of ϵ_r was due to the uniform grain size and the regular, as well as easy movement of domain walls [37]. For these reasons, ϵ_r of Fig. 6c at low frequencies was entirely higher than others and, by contrary, the dielectric loss was also relatively low in these patterns. In order to investigate the theoretical basis on the evolution of ϵ_r and $\tan \delta$, the temperature dependence of permittivity was shown in Fig. 7. The sharp permittivity peaked at pH 5, whose permittivity had achieved peak value ($\epsilon_r = 8113.81$, $T_c = 59^\circ\text{C}$) accompanied with low dielectric loss and ferroelectric–paraelectric phase transformation temperature (T_c). Moreover, the permittivity peak of pH 3, 4, 6, 7, and 8 phase transition temperature range became broader, meaning the diffuse phase transition. As a typical characteristic of the relaxor ferroelectrics, the relaxor behavior due to the diffuse phase transition, which is engendered by polar-regions local spontaneous polarization [38, 39]. The phenomenon of polar-regions local spontaneous polarization at paraelectric phase was called polar nanoregions. Further, the disordered morphology and the expanded grain size of ceramics could produce polar nanoregions [39]. Consequently, the ceramics synthesized by the gel with different pH conditions ultimately led to the evolution of permittivity. In conclusion, the structural uniformity in ceramic at pH 5 really contributed to the dielectric property. These results essentially corresponded to the interrelationship of morphology and electrical properties as mentioned before.

The d_{33} , k_p , and Q_m of BST ceramics were shown in Fig. 8. As the increment of pH values, the d_{33} values decreased first, then reached a peak value 78 pC/N, and eventually decreased again. BST ceramics were poled in silicon oil by dc field 3 kV for 40 min under the room temperature; thus, the d_{33} value was affected by poling levels first [37].

From the figure, the relatively smaller d_{33} of BST ceramic was obtained with the larger grain size, which was in line with the literature reported by Shao et al. [40]. The k_p values almost decreased with the increment of the pH conditions. The optimal planar electromechanical property achieved at

pH 5 with $k_p = 14.96\%$ when pH conditions ranged from 4 to 8. However, the optimal k_p values was obtained at pH 3 when pH conditions ranged from 3 to 8. It was because the highest density of these ceramics is speculated with the optimal k_p values [40]. The Q_m values increased sostenuto at pH 3–5 and decreased at pH 6–8. The growth in grain size engendered the intensive strain in domain movement, and ulteriorly in the increment of Q_m values [41]. Thus, we could conclude that the optimal d_{33} value was 78 pC/N, Q_m was 236.43, and the k_p was 14.96% at pH 5.

4 Conclusion

BST nanopowders were calcined under different temperatures and the BST ceramics were synthesized with gels at pH 3–8. The BaCO₃ impurity phase in BST nanopowder was detected under the temperature of 440 °C and disappeared under the temperature of 800 °C. The precipitation phase had an adverse effect on the electrical properties and morphologies, which were brought by the gels with different pH conditions. The optimal electrical properties of the BST ceramics were obtained, i.e., $\epsilon_r = 8113.81$, $d_{33} = 78$ pC/N, $k_p = 14.96\%$, and $Q_m = 85.08$ at pH 5. The interrelationship between the morphology and optimal electrical property of BST ceramics was also analyzed. The uniform population of domains and regular grain size as well as the distinct phase boundaries led to the increment in permittivity and d_{33} . In addition, the excellent electrical properties of BST ceramics in this work could be used in the tunable microwave applications.

Acknowledgements We thank the Henan Provincial Department of Science and Technology Research Project (162102310122), the Key Project of Henan Province Colleges and Universities (19A430021), the Scientific Research Foundation of Graduate School of Xinyang Normal University (2018KYJJ17), and Nanhu Scholars Program for Young Scholars of XYNU, for their financial support.

Compliance with ethical standards

Conflict of interest The authors declare that they have no conflict of interest.

Publisher's note: Springer Nature remains neutral with regard to jurisdictional claims in published maps and institutional affiliations.

References

- Mondal T, Majee BP, Das S, Sinha TP, Middy TR, Badapanda T, Sarum PM (2017) A comparative study on electrical conduction properties of Sr-substituted Ba_(1-x)Sr_xZr_{0.1}Ti_{0.9}O₃ (x=0.00–0.15) ceramics. *Ionics* 23:2405–2416
- Bian Y, Zhai J (2014) Low dielectric loss Ba_{0.6}Sr_{0.4}TiO₃/MgTiO₃ composite thin films prepared by a sol-gel process. *J Phys Chem Solids* 75:759–764
- Stanculescu R, Ciomaga CE, Padurariu L, Galizia P, Horchidan N, Capiani C, Galassi C, Mitoseriu L (2015) Study of the role of porosity on the functional properties of (Ba,Sr)TiO₃ ceramics. *J Alloy Compd* 643:79–87
- Upadhyay RB, Annam S, Patel MR, Sharma AK, Mevada P, Joshi US (2016) Ba_{0.60}Sr_{0.4}TiO₃ thick film derived by polymer modified MOSD route for tunable micro strip antenna applications. *Ferroelectr Lett* 43:25–33
- Upadhyay RB, Annam S, Patel MR, Joshi US (2015) Influence of aliovalent doping on dielectric properties of Ba_{0.6}Sr_{0.4}TiO₃ thin film for voltage tunable applications. *Integr Ferroelectr* 167:184–191
- Li Y, Cheng HB, Xu HW, Zhang YX, Yan P, Huang T, Wang CM, Hu ZG, Ouyang J (2016) Electromechanical properties of (Ba,Sr)(Zr,Ti)O₃ ceramics. *Ceram Int* 42:10191–10196
- Pal J, Kumar S, Singh L, Singh M, Singh A (2017) Detailed investigation on structural, dielectric, magnetic and magnetodielectric properties of BiFeO₃-BaSrTiO₃ solid solutions. *J Magn Magn Mater* 441:339–347
- Hossain SKS, Roy PK (2017) Structural and electro-magnetic properties of low temperature co-fired BaSrTiO₃ and NiCuZn ferrite composites for EMI filter applications. *J Mater Sci Mater El* 28:18136–18144
- Li P, Zhai JW, Shen B, Zhang SJ, Li XL, Zhu FY, Zhang XM (2018) Ultrahigh piezoelectric properties in textured (K,Na)NbO₃-Based lead-free ceramics. *Adv Mater* 30:1705171
- Tian YS, Gong YS, Meng DW, Deng H, Kuang BY (2015) Low-temperature sintering and electric properties of BCT-BZT and BCZT lead-free ceramics. *J Mater Sci Mater El* 26:3750–3756
- Dong SP, Rao AVP, Komarneni S (1997) Titanate and barium/strontium titanate thin films from hydroxide precursors: preparation and ferroelectric behavior. *J Sol Gel Sci Techn* 10:213–220
- Huang YH, Wu YJ, Li J, Liu B, Chen XM (2017) Enhanced energy storage properties of barium strontium titanate ceramics prepared by sol-gel method and spark plasma sintering. *J Alloy Compd* 701:439–446
- Gharibshahian M, Nourbakhsh MS, Mirzaee O (2018) Evaluation of the superparamagnetic and biological properties of microwave assisted synthesized Zn & Cd doped CoFe₂O₄ nanoparticles via Pechini sol-gel method. *J Sol Gel Sci Techn* 85:684–692
- Salavati-Niasari M, Soofivand F, Sobhani-Nasab A, Shakouri-Arani M, Hamadani M, Bagheri S (2017) Facile synthesis and characterization of CdTiO₃ nanoparticles by Pechini sol-gel method. *J Mater Sci Mater El* 28:684–692
- Danks AE, Hall SR, Schnepf Z (2016) The evolution of 'sol-gel' chemistry as a technique for materials synthesis. *Mater Horiz* 3:91–112
- Suárez-Toriello VA, Santolalla-Vargas CE, Reyes JADL, Vázquez-Zavala A, Vrinat M, Geantet C (2015) Influence of the solution pH in impregnation with citric acid and activity of Ni/W/Al₂O₃ catalysts. *J Mol Catal A Chem* 404–405:36–46
- Zheng T, Ding Y, Wu JG (2006) Bi nonstoichiometry and composition engineering in (1-x)Bi_{1+y}FeO_{(3+3y)/2}-xBaTiO₃ ceramics. *RSC Adv* 6:90831–90839
- Onoe M, Jumonji H (1966) Useful formulas for piezoelectric ceramic resonators and their application to measurement of parameters. *J Acoust Soc Am* 41:1223–1223
- Danish M, Ambreen S, Chauhan A, Pandey A (2015) Optimization and comparative evaluation of optical and photo catalytic properties of TiO₂ thin films prepared via sol-gel method. *J Saudi Chem Soc* 19:557–562

20. Wu YT, Wang XF, Yu CL, Li EY (2012) Preparation and characterization of barium titanate (BaTiO_3) nano-powders by Pechini sol-gel method. *Adv Manuf Process* 27:1329–1333
21. Hsieh TH, Yen SC, Ray DT (2012) A study on the synthesis of $(\text{Ba,Ca})(\text{Ti,Zr})\text{O}_3$ nano powders using Pechini polymeric precursor method. *Ceram Int* 38:755–759
22. Maya JC, Chejne F, Bhatia SK (2016) Novel model for the sintering of ceramics with bimodal pore size distributions: application to the sintering of lime. *AIChE J* 63:893–902
23. Hasbullah NN, Lee OJ, Chyi JLY, Chen SK, Talib ZA (2017) Synthesis of BaTiO_3 nanoparticles via hydrothermal method. *Solid State Phenom* 268:172–176
24. Jayalath S, Wu H, Larsen SC, Grassian VH (2018) Surface adsorption of suwannee river humic acid on TiO_2 nanoparticles: a study of pH and particle size. *Langmuir* 34:3136–3145
25. Peperstraete Y, Amzallag E, Tetot R, Pascale R (2018) Ab initio study for the IR spectroscopy of PbTiO_3 and PbZrO_3 , primary blocks of $\text{PbZr}_{1-x}\text{Ti}_x\text{O}_3$. *J Phys-Condens Mat* 30:1–11
26. Hao YN, Wang XH, Kim JY, Li LT (2014) Rapid formation of nanocrystalline BaTiO_3 and its highly stable sol. *J Am Ceram Soc* 97:3434–3441
27. Naeem A, Mahmood A, Iqbal Y, Ullah A, Mahmood T, Humayun H (2015) Dielectric and impedance spectroscopic studies on $(\text{Ba}_{0.5}\text{Sr}_{0.5})\text{Mn}_x(\text{Ti}_{0.95}\text{Fe}_{0.05})_{1-x}\text{O}_3$ ceramics synthesized by using sol-gel method. *J Alloy Compd* 645:290–296
28. Attar AS, Sichani ES, Sharafi S (2016) Structural and dielectric properties of Bi-doped barium strontium titanate nanopowders synthesized by sol-gel method. *J Mater Res Technol* 6:108–115
29. Lopes CDCA, Limirio PHJO, Novais VR, Dechichi P (2018) Fourier transform infrared spectroscopy (FTIR) application chemical characterization of enamel, dentin and bone. *Appl Spectrosc Rev* 53:1–23
30. Liu SZ, Wang TX, Yang LY (2011) Low temperature preparation of nanocrystalline SrTiO_3 and BaTiO_3 from alkaline earth nitrates and TiO_2 nanocrystals. *Powder Technol* 212:378–381
31. Raj R, Ashby MF (1975) Intergranular fracture at elevated temperature. *Acta Metall Sin* 23:653–666
32. Ortiz M, Suresh S (1993) Statistical properties of residual stresses and intergranular fracture in ceramic materials. *J Appl Mech* 60:77–84
33. Han XH, Li Y, Zhao YQ, Chi X, Zhang C, Bian LP, Sun JB, Zhang Y (2017) Microstructure and phase transition of Fe-24Cr-12Co-1.5Si ribbons. *J Alloy Compd* 731:10–17
34. Huang YQ, Du HW, Feng W, Qin HN, Hu QB (2014) Influence of SrZrO_3 addition on structural and electrical properties of $(\text{K}_{0.45}\text{Na}_{0.51}\text{Li}_{0.04})(\text{Nb}_{0.90}\text{Ta}_{0.04}\text{Sb}_{0.06})\text{O}_3$ lead-free piezoelectric ceramics. *J Alloy Compd* 590:435–439
35. Srikanth KS, Singh VP, Vaish R (2017) Pyroelectric performance of porous $\text{Ba}_{0.85}\text{Sr}_{0.15}\text{TiO}_3$ ceramics. *Int J Appl Ceram Tec* 15:140–147
36. Shaw TM, Trolier-Mckinstry S, McIntyre PC (1983) The properties of ferroelectric films at small dimensions. *Annu Rev Mater Res* 30:263–298
37. Mudinepalli VR, Feng L, Lin WC, Murty BS (2015) Effect of grain size on dielectric and ferroelectric properties of nanostructured $\text{Ba}_{0.8}\text{Sr}_{0.2}\text{TiO}_3$ ceramics. *J Adv Ceram* 4:46–53
38. Gao WW, Lv J, Lou XJ (2018) Large electric-field-induced strain and enhanced piezoelectric constant in CuO modified BiFeO_3 - BaTiO_3 ceramics. *J Am Ceram Soc* 101:2653–2665
39. Cheng S, Zhang BP, Zhao L, Wang KK (2018) Enhanced insulating and piezoelectric properties of 0.7BiFeO_3 - 0.3BaTiO_3 lead-free ceramics by optimizing calcination temperature: analysis of Bi^{3+} volatilization and phase structures. *J Mater Chem C* 6:3982–3989
40. Shao SF, Zhang JL, Zhang Z, Zheng P, Zhao ML, Li JC, Wang CL (2009) High piezoelectric properties and domain configuration in BaTiO_3 ceramics obtained through the solid-state reaction route. *J Phys D Appl Phys* 42:9801–189801
41. Liu YW, Pu YP (2016) Dielectric properties, relaxor behavior and temperature stability of $(1-x)(\text{K}_{0.4425}\text{Na}_{0.52}\text{Li}_{0.0375})(\text{Nb}_{0.87}\text{Ta}_{0.06}\text{Sb}_{0.07})\text{O}_3$ - $x\text{Ba}_{0.4}\text{Sr}_{0.6}\text{TiO}_3$ ceramics. *J Alloy Compd* 693:118–125